International Telecommunication Union

ITU-R

Radiocommunication Sector of ITU

Report ITU-R SA.2166
(09/2009)

Examples of radiation patterns of large antennas used for space research and radio astronomy

SA Series

Space applications and meteorology

International Telecommunication Union

Foreword

The role of the Radiocommunication Sector is to ensure the rational, equitable, efficient and economical use of the radio-frequency spectrum by all radiocommunication services, including satellite services, and carry out studies without limit of frequency range on the basis of which Recommendations are adopted.

The regulatory and policy functions of the Radiocommunication Sector are performed by World and Regional Radiocommunication Conferences and Radiocommunication Assemblies supported by Study Groups.

Policy on Intellectual Property Right (IPR)

ITU-R policy on IPR is described in the Common Patent Policy for ITU-T/ITU-R/ISO/IEC referenced in Annex 1 of Resolution ITU-R 1. Forms to be used for the submission of patent statements and licensing declarations by patent holders are available from http://www.itu.int/ITU-R/go/patents/en where the Guidelines for Implementation of the Common Patent Policy for ITU-T/ITU-R/ISO/IEC and the ITU-R patent information database can also be found.

Series of ITU-R Reports

(Also available online at http://www.itu.int/publ/R-REP/en)

Series	Title
BO	Satellite delivery
BR	Recording for production, archival and play-out; film for television
BS	Broadcasting service (sound)
BT	Broadcasting service (television)
F	Fixed service
M	Mobile, radiodetermination, amateur and related satellite services
P	Radiowave propagation
RA	Radio astronomy
RS	Remote sensing systems
S	Fixed-satellite service
SA	**Space applications and meteorology**
SF	Frequency sharing and coordination between fixed-satellite and fixed service systems
SM	Spectrum management

***Note**: This ITU-R Report was approved in English by the Study Group under the procedure detailed in Resolution ITU-R 1.*

Electronic Publication
Geneva, 2010

REPORT ITU-R SA.2166

Examples of radiation patterns of large antennas used for space research and radio astronomy

(2009)

TABLE OF CONTENTS

FIGURES

Page

TABLES

1 Introduction

The methodology and guidelines introduced in § 2 have been used to model the radiation patterns for large antennas used in deep space research and radio astronomy. These methods are described in detail in Recommendation ITU-R SA.1345 – Methods for predicting radiation patterns of large antennas used for space research and radio astronomy.

In predicting the radiation pattern of the NASA's deep space network (DSN) antenna, the latest version of a commercially available software package (GRASP9) has been used. For the radiation pattern of the radio astronomy antenna, an old version (GRASPC) of the same software has been used. The results illustrate the effect of various parameters on the model's predictions and the significance of various mechanical and design features.

2 Model methodology

The GRASP9/GRASPC is based on well-established analysis techniques of physical optics (PO), supplemented with physical theory of diffraction (PTD), geometrical optics (GO), and uniform geometrical theory of diffraction (GTD). Geometrical optics and GTD are ray-based analysis methods which can only be applied to one single reflector at a time to limit the complexity of the associated ray-tracing problem. Physical optics and PTD can be applied to any number of reflector analyses in arbitrary order, where the induced currents obtained by a physical optics analysis on one reflector can be used as a source illuminating a second reflector.

For the physical optics calculations, the surface of the reflector is divided into a grid of surface elements. The radiated field is found by integration of the surface currents at each point on the grid. To simulate the effect of aperture blockage, the surface currents are set to zero in the shadow of the feed on the reflector surface.

The GTD approach follows three steps:

Step 1: selection of significant rays;

Step 2: ray tracing;

Step 3: field calculation.

A simple caustic correction procedure is applied which smoothes the diffracted field for angles close to the caustic direction. It cannot, however, accurately predict the field close to the caustic in the boresight direction. The GTD method, in general, requires less computation time than the physical optics approach. Therefore, GTD is used for all angles except where GTD is inaccurate. Due to the caustic on boresight, the physical optics method is used for angles in this sector.

The scattering effects from supporting struts are determined by means of physical optics. For thick struts the conventional physical optics approach is used, and for thin struts a special technique is developed which makes it possible to calculate the surface currents on both the illuminated and the shadow side of the strut.

Two important effects from struts are typical for reflector antennas:

1 they may block the field from the main reflector travelling towards the far field;

2 they may shadow the field from the feed illuminating the reflector.

Both of these effects may be calculated in GRASP9.

Random surface distortions can be imposed on the surface of the main reflector. The distortions are correlated over a distance consistent with the size of the individual panels of the reflector surface.

2.1 Guidelines on selecting physical optics-PTD or geometrical optics-GTD

Physical optics-PTD and geometrical optics-GTD can be used as alternative analysis methods, except for the main-beam direction of a focusing aperture where GTD fails. The analysis method applied to a particular problem depends on many factors. Typically, physical optics should be used in the following cases:

1 the field is calculated at or near a caustic of the reflected field, i.e. in the focusing region of a reflector;

2 the reflector is in the near field of the feed, (in contrast, GTD always assumes far-field conditions);

3 the antenna is a dual-reflector system with low cross-polarization requirement, since physical optics is more accurate in predicting the cross-polarization due to the sub-reflector curvature;

4 the reflector is shaped, (in this case the GTD algorithm may not find all diffraction points and there may be more reflection points for one field point);

5 the reflector has an irregular edge, (in this case the GTD ray tracing algorithm may fail in finding all diffraction points, just as the inclusion of a corner-diffracted field may be necessary to obtain satisfactory accuracy, an option which is not included in GRASP9).

On the other hand, GTD may be more appropriate for the following cases:

1 the antenna has a single electrically large reflector, and the radiation pattern is calculated for a wide range of angles, since the physical optics analysis may take substantially longer than the GTD analysis, especially for higher frequencies (larger antenna size in terms of wavelength). This is due to the fact that many more field point calculations are necessary to sample the far-field sufficiently and accurately, and each field point calculation would require substantially higher number of current integration points. A GTD analysis does not suffer from the second factor since it is almost independent of the antenna size;

2 the near-field pattern needs to be calculated quickly, and where it can provide insight into a particular scattering problem if the edge-diffracted and reflected ray fields are observed independently.

2.2 Analysis of struts

In single and dual reflector antennas, struts are used to support the feed system and sub-reflector in rotationally symmetric or near-symmetric systems. These struts may have a serious impact on the antenna performance. The efficiency and cross-polarization are degraded and the side-lobe level is increased. The three most important mechanisms by which the strut scattering influences the antenna radiation are:

1 shadowing and changes of the main reflector currents caused by direct feed illumination of the struts;

2 shadowing and changes of the main reflector field by the struts and consequent reflector field blockage effects;

3 reflected field from the main reflector by the scattered field from the struts, which originated from the incident field on the strut from the main reflector.

The degradation of the peak gain (efficiency) is mainly due to the effects (1) and (2) of which (1) is only important in a system where the struts are not supported by the outer edge of the main reflector. The side-lobes will mainly be affected by the strut scattering (2) and (3) where (3) is rarely significant and occurs in very special cases.

For circular struts, two types of analyses can be used depending on the size of the struts:

1 a simple physical optics approach, which is especially useful for struts which are thick relative to the wavelength;

2 a canonical solution for struts with diameters in the order of the wavelength.

An accurate prediction of the effects of the struts both on the main lobe and on the side-lobes can be achieved by taking the current distribution along the circumference of the strut into account. This is relatively simple for a circular strut, because the canonical problem (plane wave incidence on an infinite circular cylinder) has a simple solution in series form. For thick struts the current distribution can alternatively be found by the simple physical optics approximation. To include the precise effect of the struts in the radiation pattern requires elaborate and time consuming computation.

3 Example: Deep space research antenna (DSN 34-m)

3.1 Antenna mechanical parameters

The major parameters of the 34-m beam-waveguide (BWG) antenna of the DSN, are given in Table 1.

TABLE 1

Parameters of 34-m BWG JPL/NASA DSN antenna

	34-m BWG antenna
Main reflector diameter	34 m, circular aperture, shaped
Subreflector diameter	3.429 m, shaped
Focal length	11.8 m, primary focus
Frequency range	8.400-8.450 GHz (rcv) 7.145-7.190 GHz (tmt) 25.5-27 GHz (rcv) 31.8-32.3 GHz (rcv) 34.2-34.7 GHz (tmt)
Feed gain pattern	Pattern equivalent to a 31 dB gain horn
Surface distortions	0.25 mm (r.m.s.)
Surface distortion correlation distance	1-2 m

A number of these antennas are located in several places around the world; specifically, in Goldstone, California; near Madrid, Spain; and near Canberra, Australia.

The far-field distances defined for these antennas at various frequencies of operation are given in Table 2.

TABLE 2

Far-field distances for the 34-m BWG JPL/NASA DSN antenna

Mode	Frequency (GHz)	Wavelength (mm)	34-m antenna	
			Mid > (km)	Far > (km)
Tmt	2.115	141.75	0.106	16
Rcv	2.295	130.63	0.109	18
Tmt	7.1675	41.83	0.159	55
Rcv	8.425	35.58	0.167	65
Tmt	34.45	8.70	0.268	266
Rcv	32.05	9.35	0.261	247

3.2 Model results without struts

The 34-m beam-waveguide antenna was modelled at both 8.425 GHz and 32.05 GHz receive frequencies in the far-field and near-field without struts. The effects of varying the observation distance within the near-field were examined as well as the effects of surface distortions.

All the results are for the antenna assumed to be transmitting with linear polarization. All patterns are for 0° azimuth plane cut with antenna pointing in 90° elevation direction. The effects of gravity, wind, etc. are ignored.

3.2.1 Far-field and near-field of 34-m antenna at 8.425 GHz (no struts)

Figures 1a) and 1b) show the gain pattern at 8.425 GHz with no surface errors and no struts in both linear and logarithmic scales.

The physical optics-PTD method was used from 0 to 0.1° (less than 2 beamwidths). The GTD-PO (GTD on subreflector, physical optics from main) was used from 0.1 to 4°. Then, geometrical optics-GTD method was used at all other angles. The three curves in the figures show the changing gain pattern as the observation point moves from far-field to successively shorter near-field distances. It should be noted that, the curve spike at around 10° is due to the feed to subreflector edge diffraction, while the spike at around 100-110° is due to the subreflector to the main reflector edge diffraction in back field region.

3.2.2 Far-field and near-field of 34-m antenna at 32.05 GHz (no struts)

Figures 2a) and 2b) show the gain pattern at 32.05 GHz with no surface distortions and no struts in both linear and logarithmic scales.

FIGURE 1

34-m antenna radiation pattern at 8.425 GHz with no surface distortion (no struts)

a) Linear angle axis

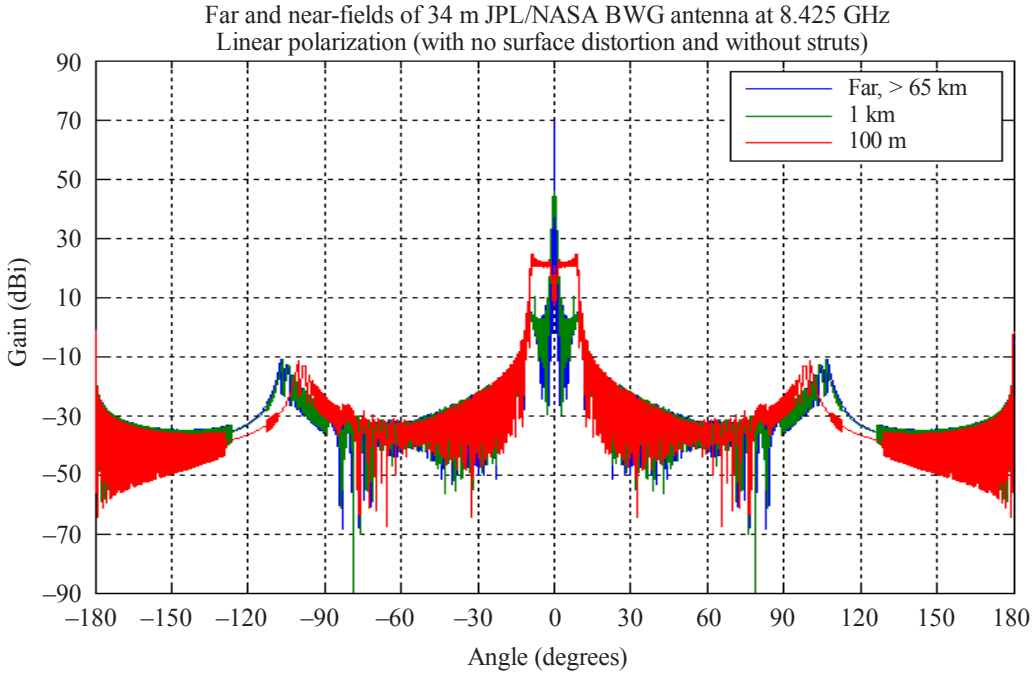

b) Logarithmic angle axis

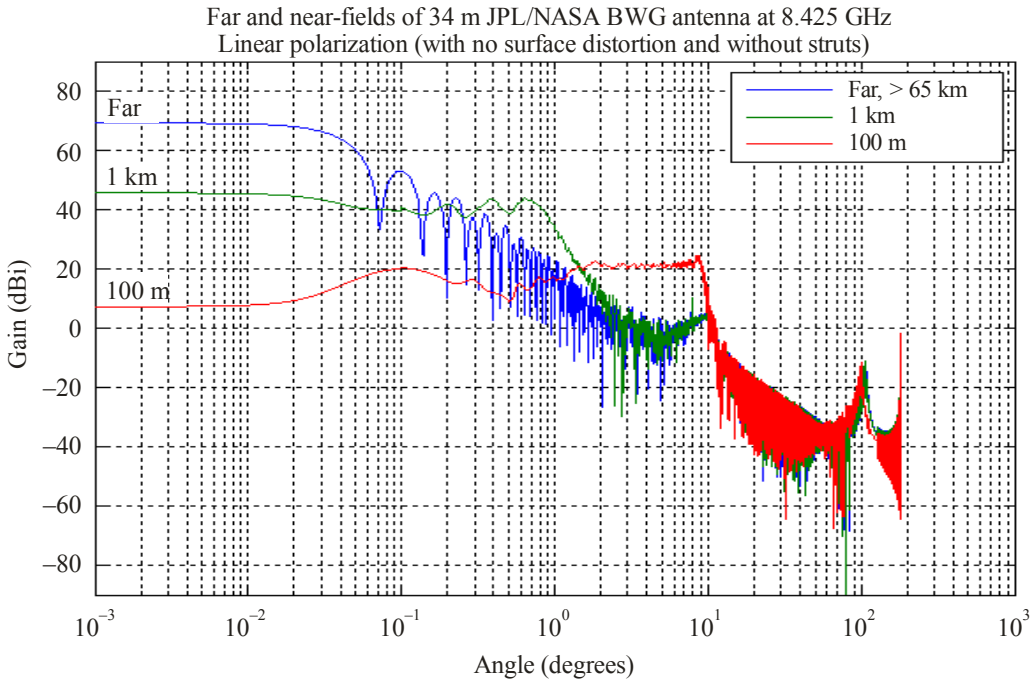

Report SA.2166-01

FIGURE 2

34-m antenna radiation pattern at 32.05 GHz with no surface distortion (no struts)

a) Linear angle axis

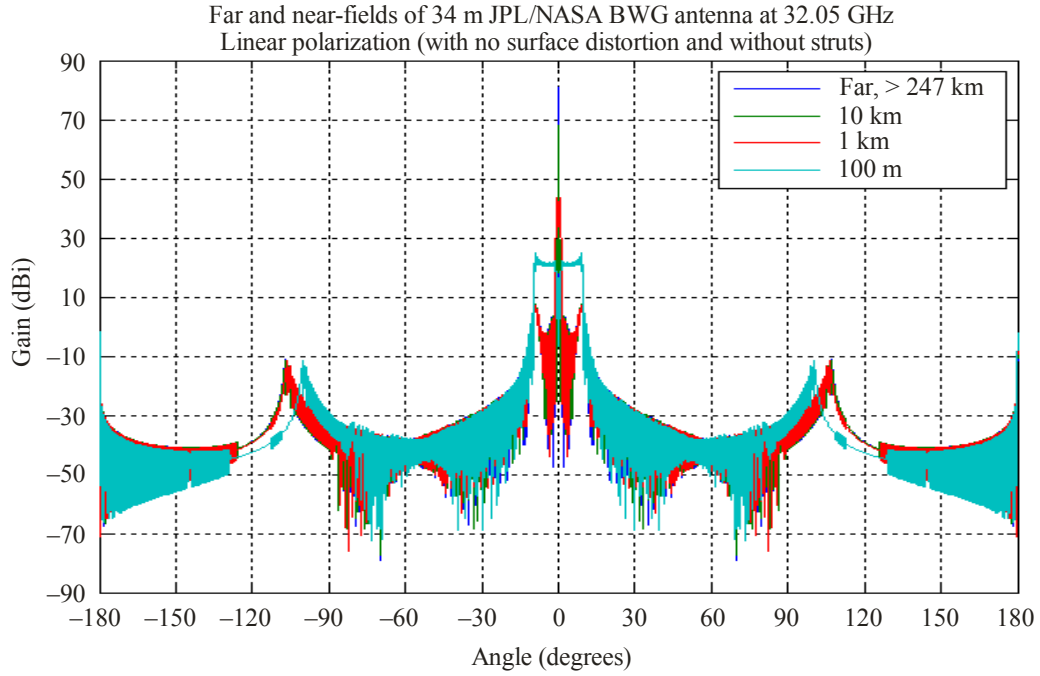

b) Logarithmic angle axis

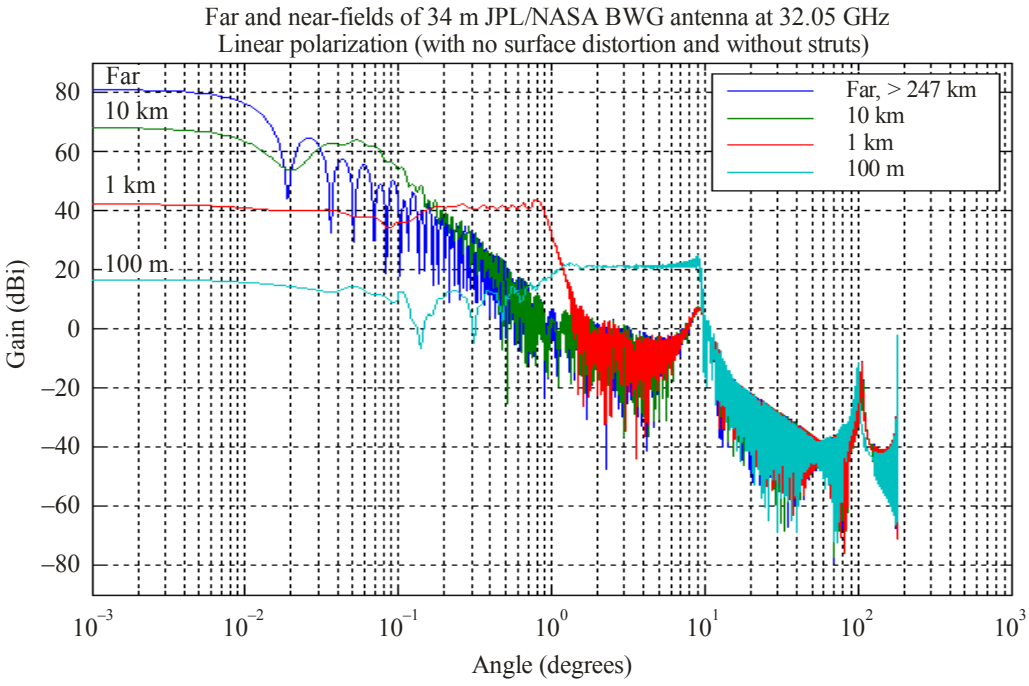

Report SA.2166-02

Again, the physical optics-PTD method was used from 0-0.1° (less than 6 beamwidths). The GTD-physical optics (GTD on subreflector, physical optics on main) was used from 0.1-4°, and geometrical optics-GTD method was used at all other angles. The four curves in the figures show the changing gain pattern as the observation point moves from far-field to successively shorter near-field distances. It should be noted that, the curve spike at around 10° is due to the feed to subreflector edge diffraction, while the spike at around 100-110° is due to the subreflector to the main reflector edge diffraction in back field region.

3.2.3 Far-field and near-field of 34-m antenna at 32.05 GHz with statistical surface distortions (no struts)

Figures 3a), 3b), 4a) and 4b) show the effect of including surface distortion by statistical approach. The nominal surface distortion of 0.25 mm is considered in Fig. 3 and 1 mm surface distortion in Fig. 4. The nominal correlation length for the errors is assumed to be 2 m, which is approximately the average size of the individual panels of the reflector surface. It can be observed that for the range of surface error and correlation lengths included, the surface distortions cause primarily to reduce the gain in the region 0-0.1° off-boresight, and there is no significant effect beyond this region.

3.3 Model results with struts

Many approximate strut representations have been introduced in the literature to calculate the effects of the struts on the field pattern. Here, a very accurate approximation is provided for the 34-m antenna with 4 struts, where each strut is represented by two metal beams with different cross sections. This is very close to the actual strut configuration, ignoring only the very thin bars connecting these two beams. Then, physical optics-PTD methods are applied to the struts.

A detailed study showed that the most significant contributions from the struts to the radiated field are due to the following components:

1 feed field to subreflector currents, then to strut currents, and finally to radiated field;

2 feed field to subreflector currents, then to main-reflector currents, then to strut currents, and finally to radiated field;

3 feed field to subreflector currents, then to strut currents, then to main-reflector currents, and finally to radiated field.

Even with the use of geometric symmetry wherever possible, the calculations are very computer-time consuming. On an average PC, calculations for the 8-GHz case can take tens of hours, and for the 32-GHz case can take hundreds of hours. Therefore, the calculations were carried out using the latest version of the GRASP software on a parallel processing supercomputer (JPL COSMOS) with 128 processors. The required time for the 8-GHz case is then reduced to about 30 min, while the 32 GHz case still takes about 20 h. By comparison, on the supercomputer, the calculation of fields in the absence of struts takes only about a minute for the 8 GHz case, and less than an hour for the 32 GHz case.

For the 32-GHz case, since the software could not perform parallelization of the PTD method for the struts, and the PTD contributions by the struts are negligible, only physical optics method was used. For the 8-GHz case, however, where the PTD contribution can be significant, physical optics-PTD methods were applied to the struts. The results showed that the struts contributed to alter the polarization of the sidelobe fields, where the cross-polarization is substantially increased for antennas with linear or circular polarizations. In addition, the co-polarization has increased by about 20 dB at 120° off-boresight for antennas with circular polarization. Below, the struts effects for far- and near-field of 34-m antenna with linear polarization are given.

FIGURE 3

34-m antenna radiation pattern at 32.05 GHz with 0.25-mm (r.m.s.) surface distortion (no struts)

a) Linear angle axis

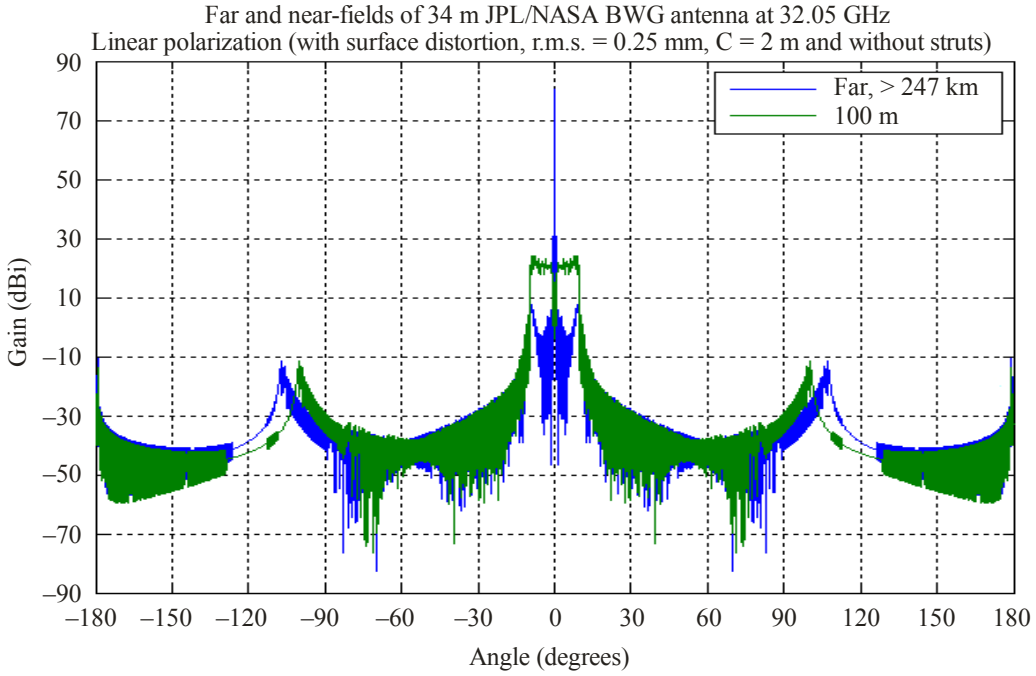

b) Logarithmic angle axis

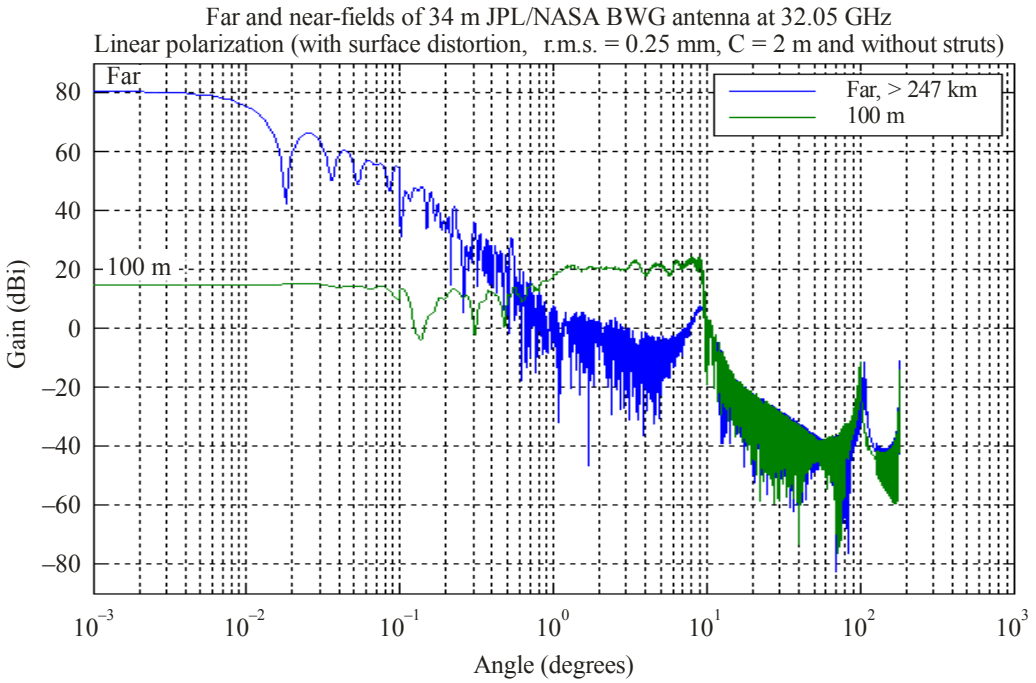

Report SA.2166-03

FIGURE 4

34-m antenna radiation pattern at 32.05 GHz with 1-mm (r.m.s.) surface distortion (no struts)

a) Linear angle axis

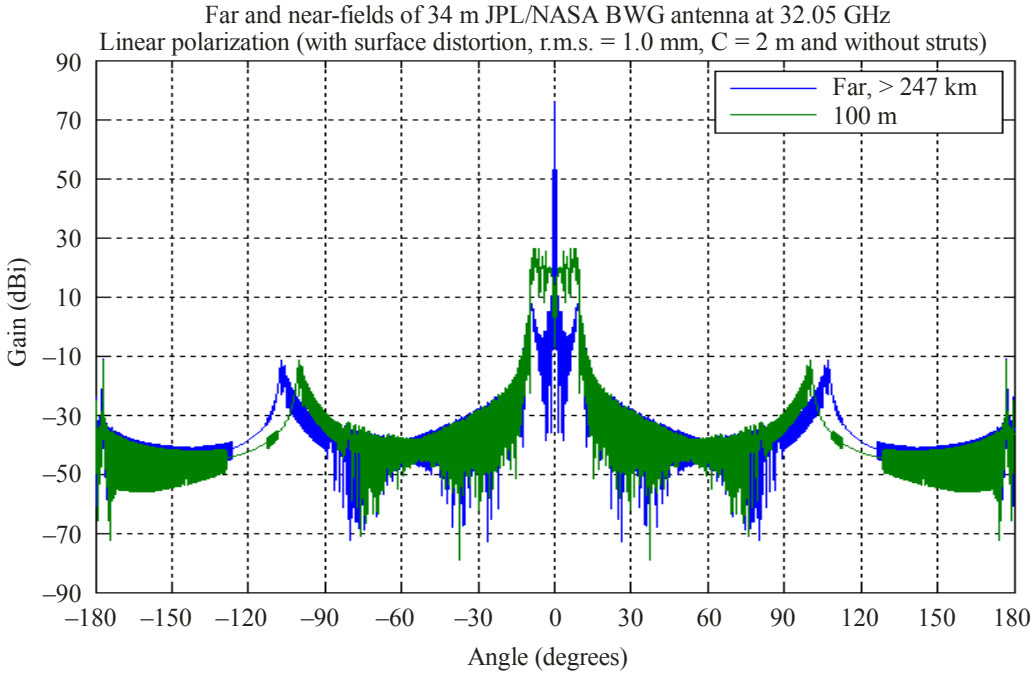

b) Logarithmic angle axis

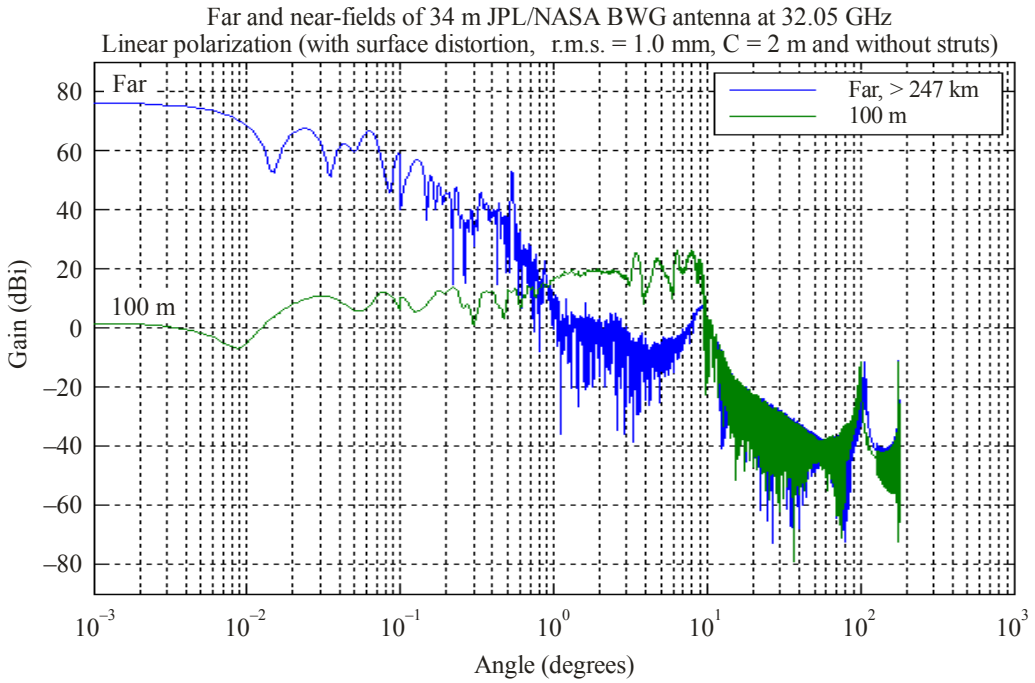

Report SA.2166-04

3.3.1 Far-field and near-field of 34-m antenna at 8.425 GHz with struts

Figures 5a) and 5b) show the gain pattern along the 0° cut at 8.425 GHz with no surface distortions, but including strut effects in linear and logarithmic scales. Figures 6a) and 6b) show the same antenna gain pattern along the 45° cut.

FIGURE 5

34-m antenna radiation pattern at 8.425 GHz with no surface distortions (with struts) (0° cut)

a) Linear angle axis

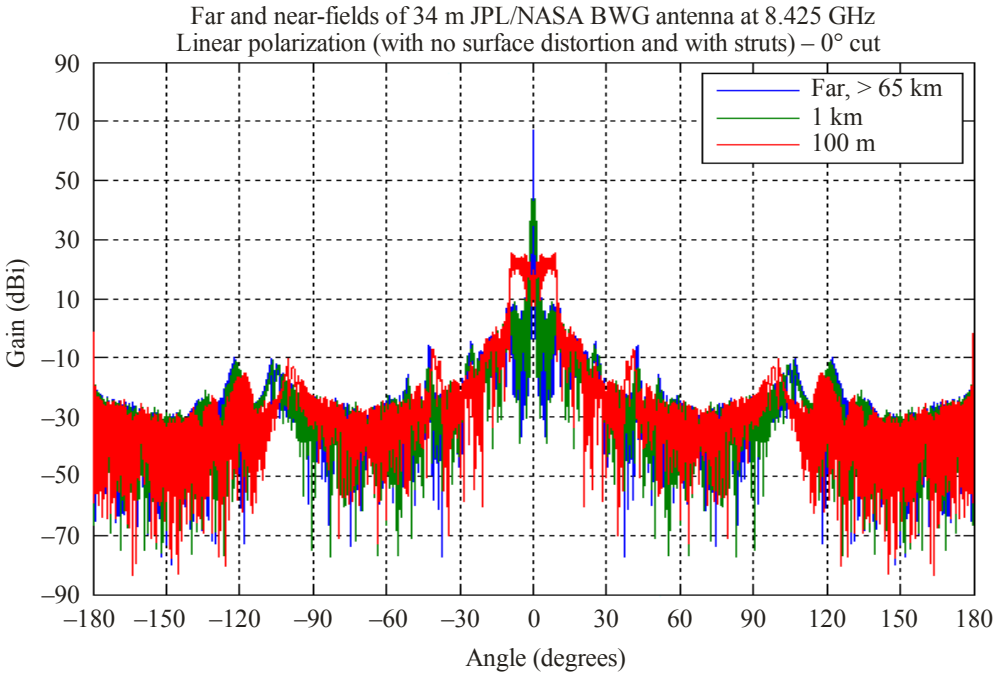

b) Logarithmic angle axis

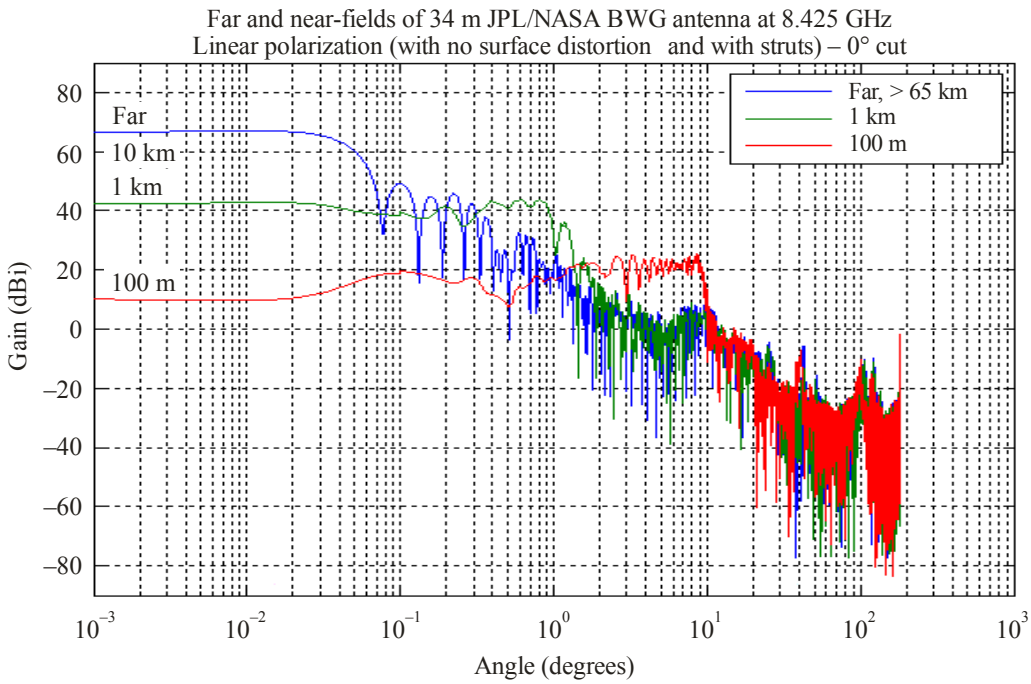

Report SA.2166-05

FIGURE 6

34-m antenna radiation pattern at 8.425 GHz with no surface distortions (with struts) (45° cut)

a) Linear angle axis

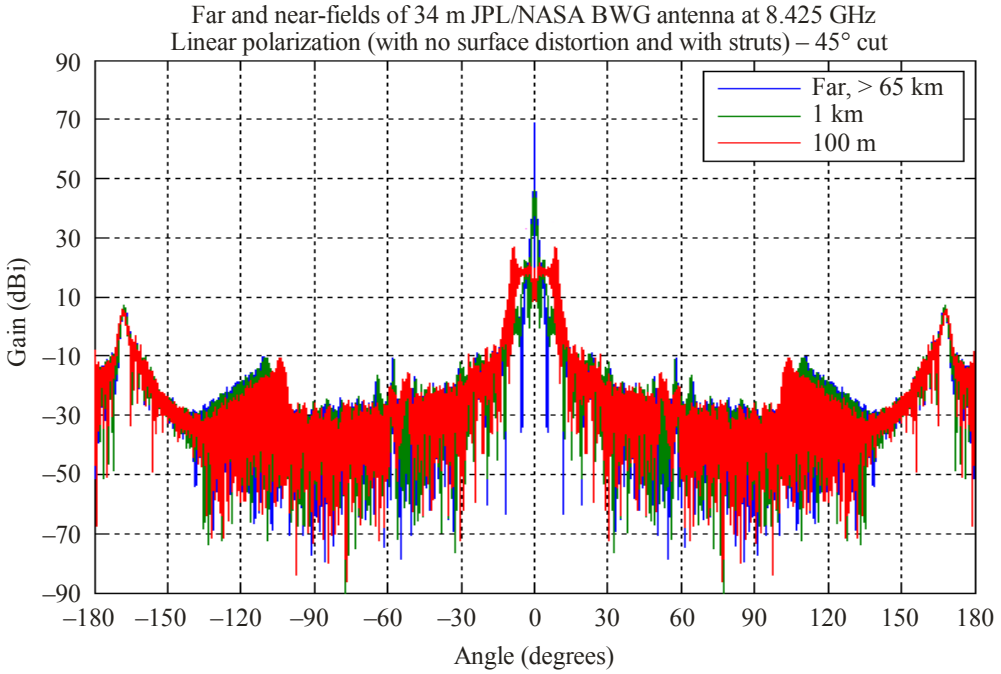

b) Logarithmic angle axis

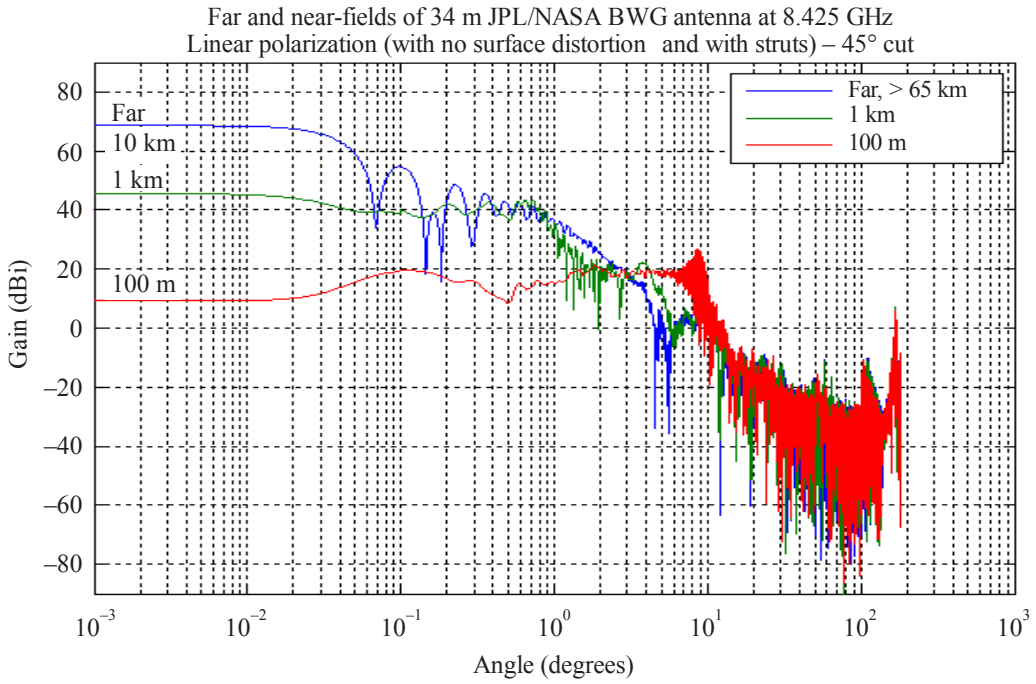

Report SA.2166-06

As seen from Figs 5 and 6, the struts create asymmetry in the radiated field pattern in different cuts around the main beam direction. This is in contrast to the relative circular symmetry of the radiated field in the no-strut case.

3.3.2 Far-field and near-field of 34-m antenna at 32.05 GHz with struts

Figures 7a) and 7b) show the gain pattern along the 0° cut at 32.05 GHz with no surface distortions, but including strut effects in linear and logarithmic scales. Figures 8a) and 8b) show the same antenna gain pattern along the 45° cut.

FIGURE 7

34-m antenna radiation pattern at 32.05 GHz with no surface distortions (with struts) (0° cut)

a) Linear angle axis

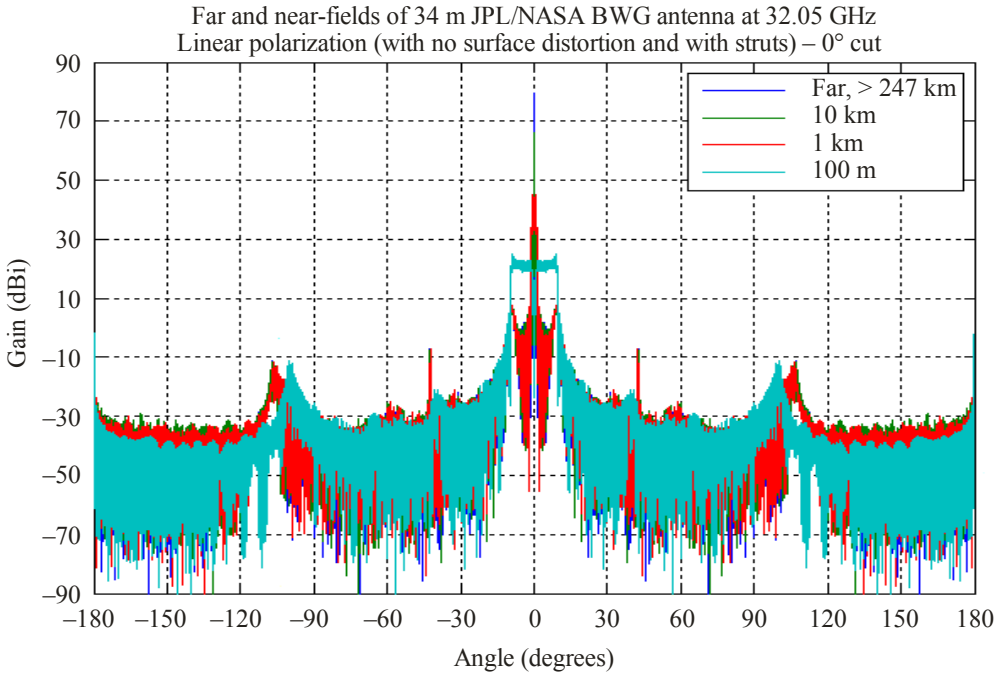

b) Logarithmic angle axis

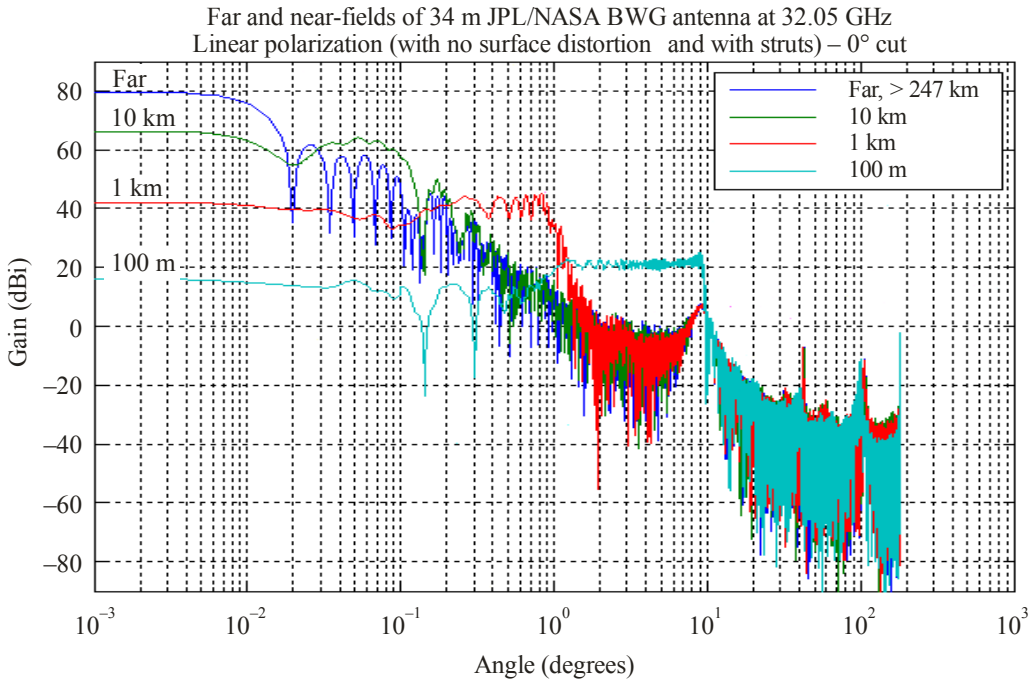

Report SA.2166-07

FIGURE 8

34-m antenna radiation pattern at 32.05 GHz with no surface distortions (with struts) (45° cut)

a) Linear angle axis

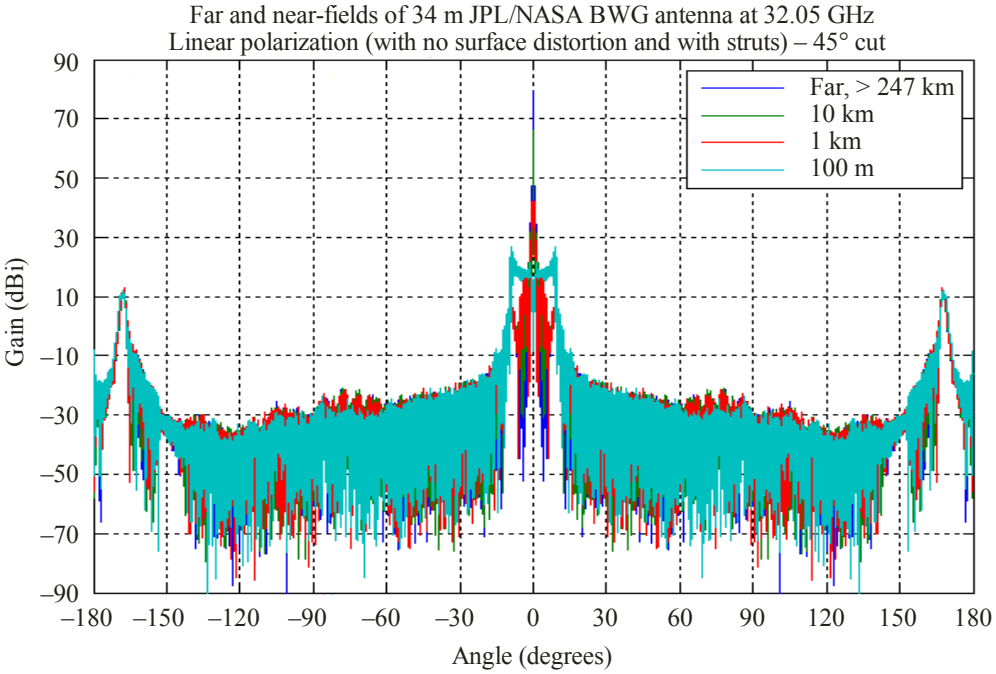

b) Logarithmic angle axis

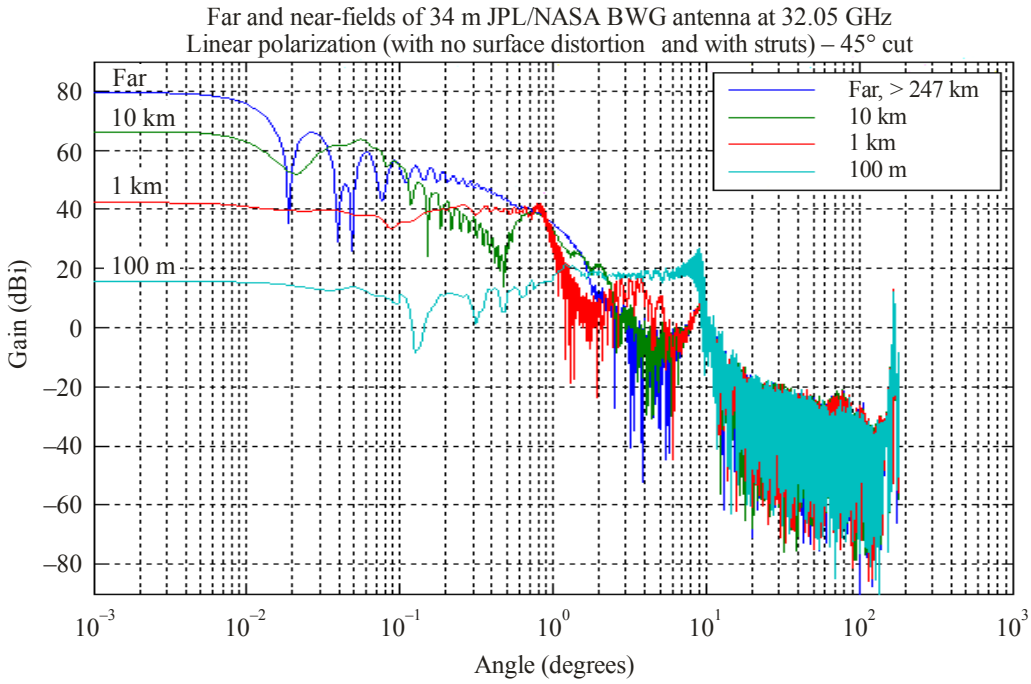

Report SA.2166-08

4 Example: Radio astronomy antenna (Lovell Mk 1A)

4.1 Antenna mechanical parameters

The Lovell Mk1A radio astronomy antenna, located at Jodrell Bank in the United Kingdom was modelled. The major parameters of this antenna are shown in Table 3.

TABLE 3

Parameters of Mk 1A radio astronomy telescope

Diameter	76.2 m, circular aperture
Focal length	22.9 m, primary focus
Frequency range	150-5 000 MHz
Support struts	The Mk 1A has a central pylon supporting the feed, this has been modelled as four individual struts, diameter 0.2 m
Feed housing	3.8 m diameter
Feed gain pattern	Parabolic, 13 dB below maximum at 59°
Surface distortions	6 mm (r.m.s.) (25 mm peak-peak)
Surface distortion correlation distance	2.8 m

4.2 Model results

The antenna was modelled at 150 MHz and at 5 000 MHz. It was modelled in the far-field, both with and without struts. The effects of varying the observation distance within the near-field were examined and the effects of surface distortions were examined.

The antenna was also modelled at the 1 420 MHz in order to compare the results with measured data taken at the same frequency.

All the results are for the Mk 1A antenna assumed to be transmitting with circular polarization. The receiver is assumed to be using vertical polarization. All patterns are for the azimuth plane, with the antenna pointing at 0° elevation.

4.2.1 Far-field and near-field at 150 MHz

Figure 9 shows the gain pattern at 150 MHz, with surface distortions included and with no struts. The physical optics method was used within 7.06° of boresight, and the GTD method at other angles. The 4 plots show the changing gain pattern as the observation point moves from far-field to successively shorter near-field distances. At this frequency, the far-field distance is 5.8 km.

It can be seen that the far-field pattern and the near-field pattern at 1 000 m are almost identical. For distances of 100 m and 50 m, the width of the main lobe increases and the maximum gain decreases. Beyond ±130°, there is little change in the level of the side-lobe envelope. At these angles the dominant rays are the edge diffracted rays.

FIGURE 9

Far- and near-field of Mk 1A at 150 MHz (no struts)

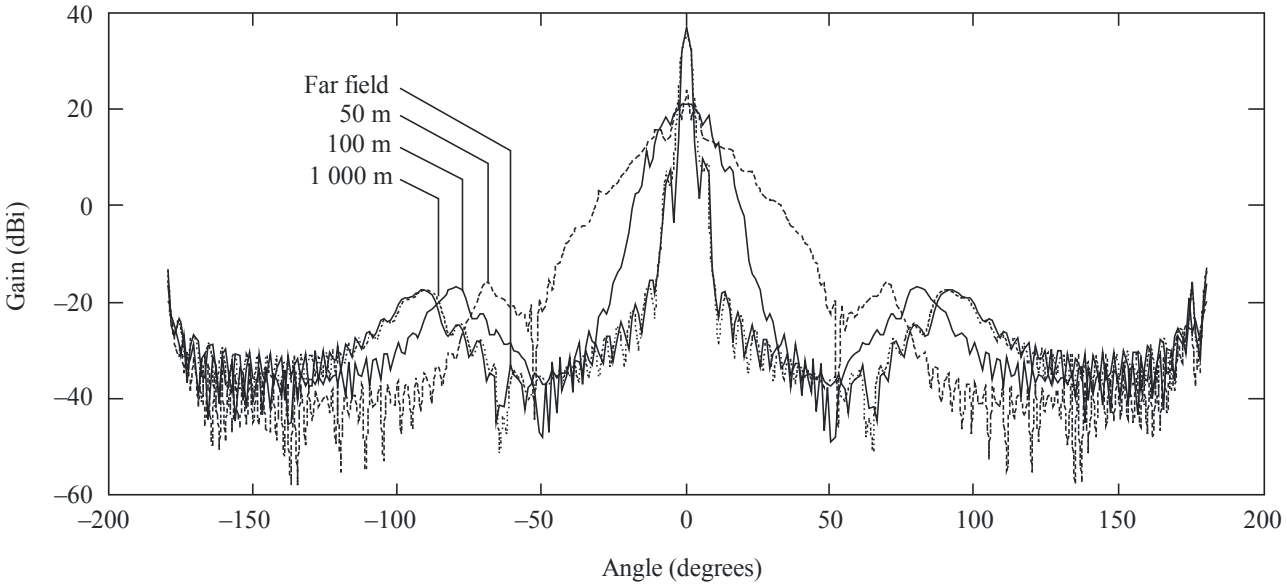

Report SA.2166-09

4.2.2 Far-field at 5 000 MHz, with and without struts

Figure 10 shows the far-field gain pattern of the Mk 1A at 5 000 MHz. Random surface distortions are included. The physical optics method was used within 0.21° of boresight, and the GTD method at other angles. One plot shows the pattern with no struts, the other has struts included. The reference radiation pattern from Recommendation ITU-R SA.509 is included.

FIGURE 10

Far-field of Mk 1A at 5 000 MHz with and without struts

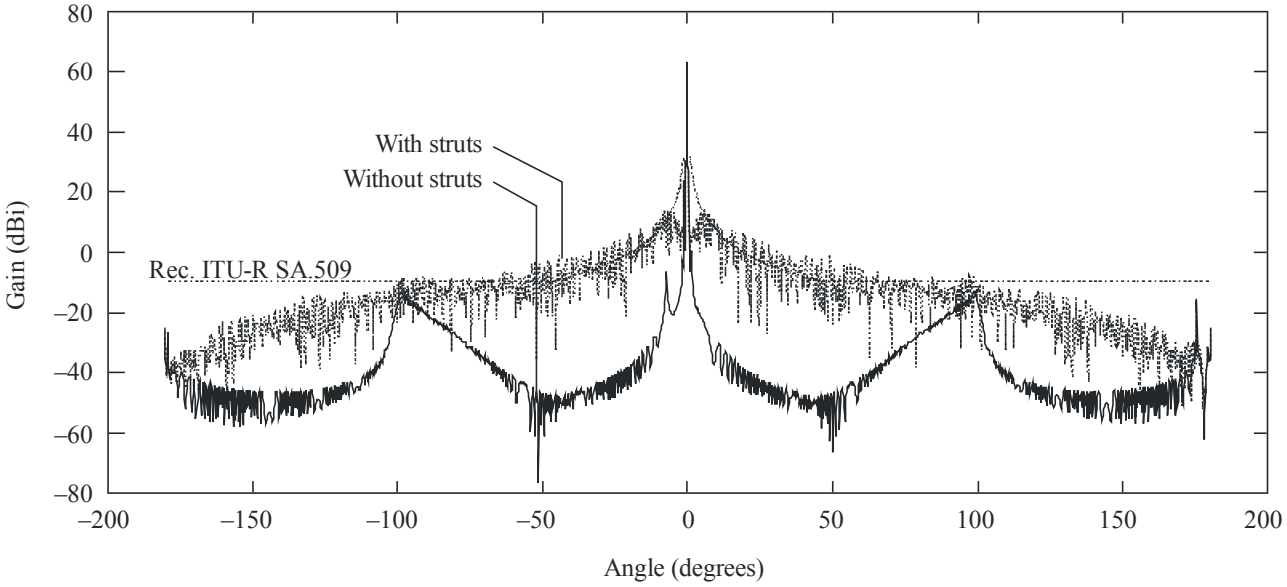

Report SA.2166-10

Without struts, the effect of spillover (radiation directly to or from the feed) is visible from the peaks at about ±100°. When struts are included, the high level of strut scattering predicted by the model tends to mask the spillover effects. With struts included, the gain pattern just exceeds the reference radiation pattern for angles less than 100° from boresight.

4.2.3 Far-field at 5 000 MHz, with and without surface distortions

Figure 11 shows the effect of using a different random number seed for the distribution of random surface deviations. Three far-field plots are shown for the MK 1A at 5 000 MHz. They are separated by 50 dB for clarity. One gives the predicted pattern with no surface distortion, the others show the effect of different random distributions. The physical optics method was used within 0.21° of boresight, and the GTD method at other angles.

FIGURE 11

Far-field at 5 000 MHz with and without surface distortion

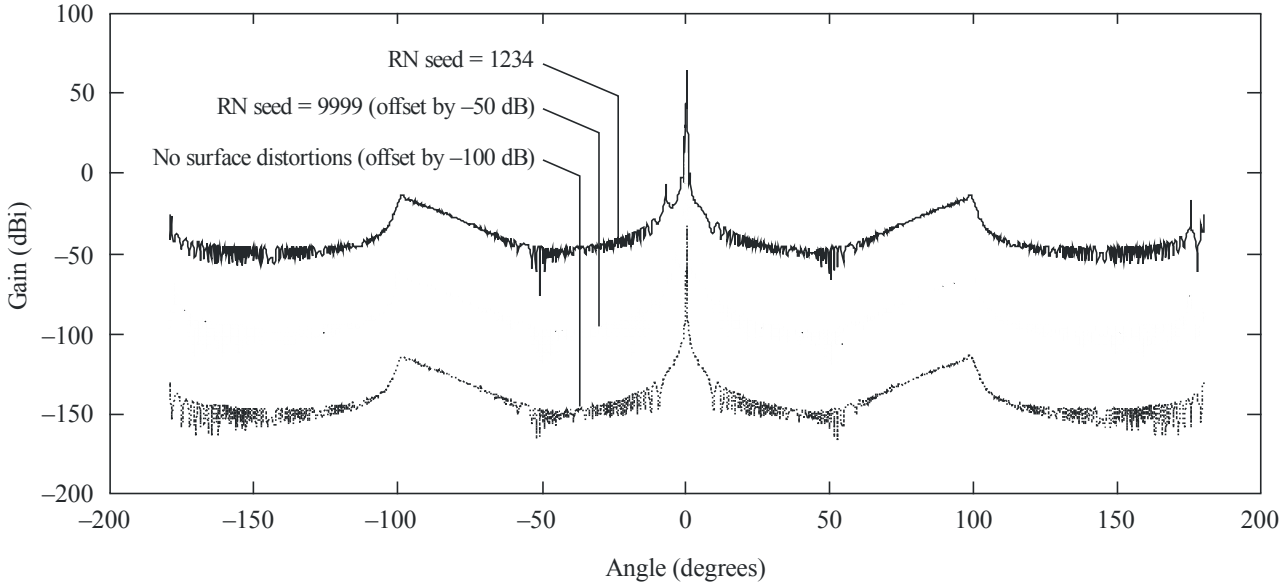

Report SA.2166-11

One can see that the surface distortions produce “spikes” near the main beam. The “spikes” are about 10 dB higher than the level with no surface distortion. Beyond about 10° from boresight, surface distortions appear to have little effect. If strut scattering were included (as indicated by Fig. 10), the “spikes” close to boresight would be masked.

4.2.4 Far-field and near-field at 5 000 MHz, without struts

Figure 12 shows the effect of viewing the antenna in the near-field. The plots are for the Mk 1A at 5 000 MHz with surface distortions, viewed from the far-field and at three different near-field distances. The physical optics method was used within 0.21° of boresight, and the GTD method at other angles. The plots are separated by 70 dB for clarity.

FIGURE 12

Far- and near-field of Mk 1A at 5 000 MHz (no struts)

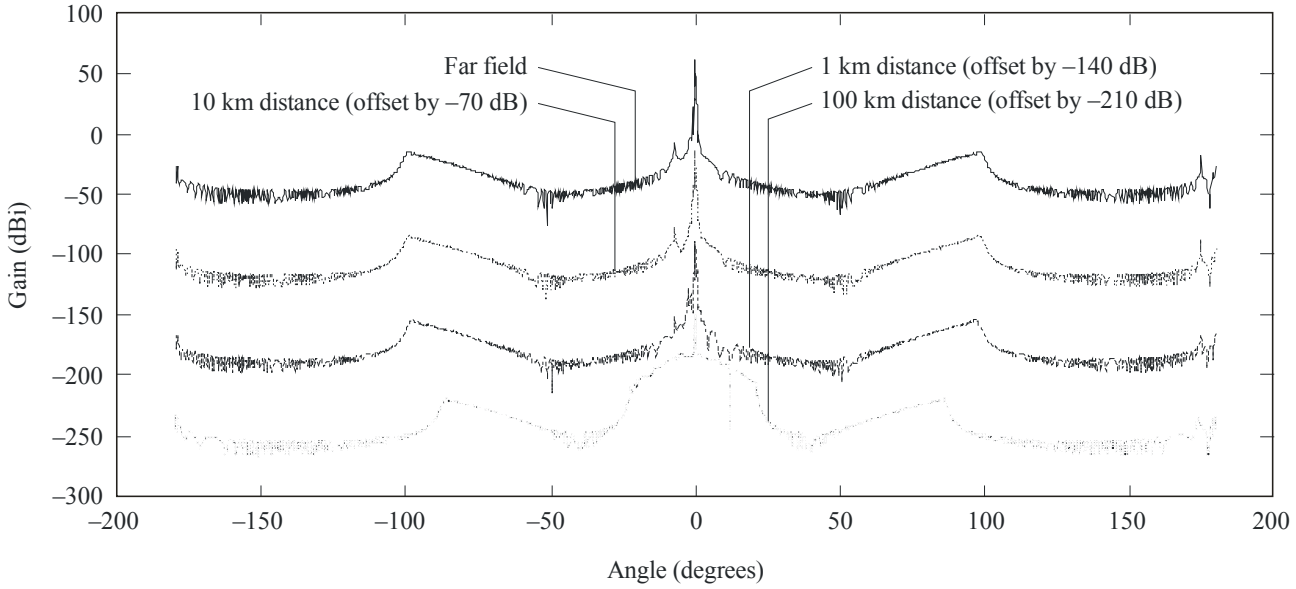

Report SA.2166-12

The prediction for a near-field distance of 10 km is almost identical to the far-field plot. At the 1 km observation distance the main beam becomes wider and the maximum gain is lowered. At 100 m the main beam is wider still and maximum gain is lowered again. Beyond ±50° there is little difference in the level of the side-lobe gain. The peaks at around 100° are due to spillover from the feed. The angle at which the spillover peaks occurs is seen to change as the observation distance is shortened. This is because the centre of the coordinate system is at the centre of the main reflector and the angle between boresight and the edge of the main reflector changes with distance.

4.2.5 Comparison of measured pattern with model prediction

Figure 13a) shows a far-field prediction for the Mk 1A at 1 420 MHz. The gain is relative to the maximum gain of 57 dBi. Figure 13b) shows the measured gain of the Mk 1A at the same frequency. The peak in the measured signal at around 95° is due to spillover.

The model appears to underestimate the level of the side lobes close to the main beam (to about 15°), and the high level of spillover. For the side-lobe level between 15° and 80°, there are a limited number of samples but the predicted level appears approximately to be correct.

FIGURE 13

Predicted and measured far-field of Mk 1A at 1 420 MHz

a) Model prediction

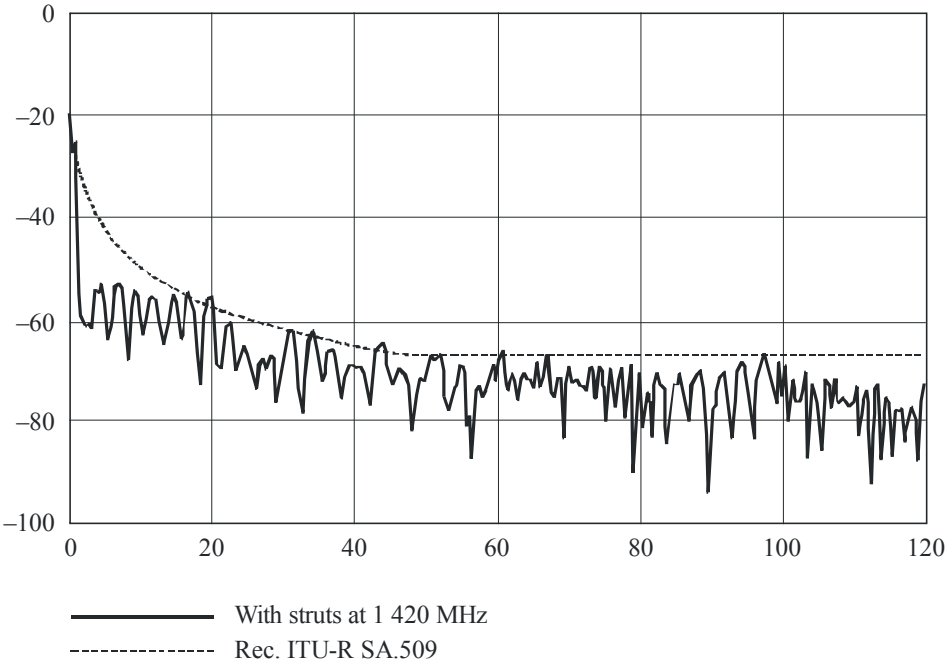

b) Measured gain

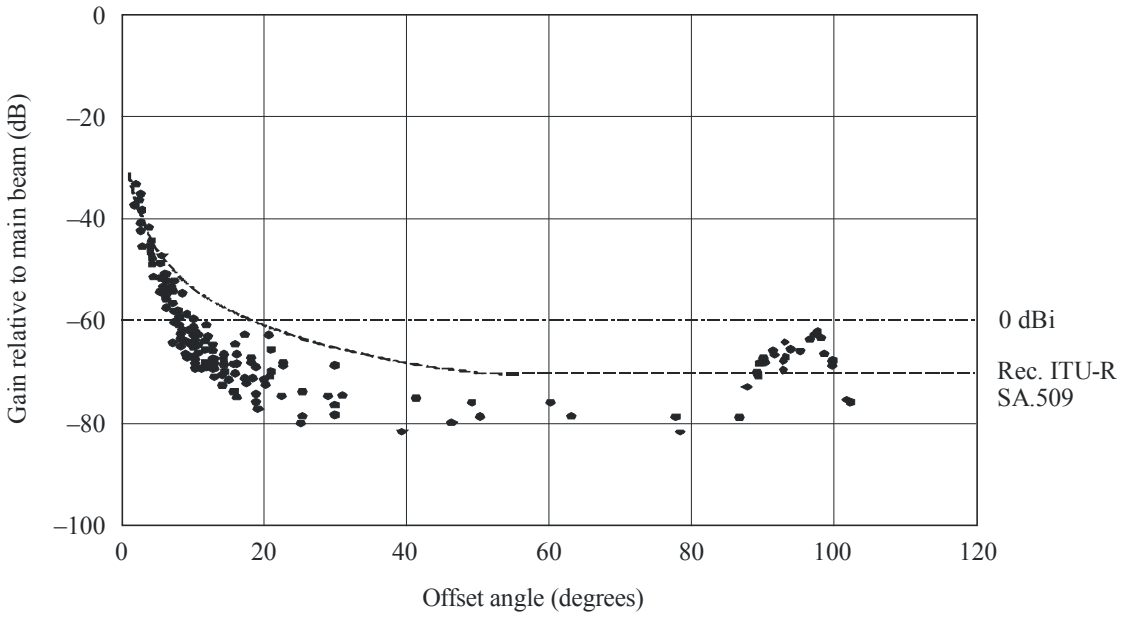

Report SA.2166-13

5 Conclusions

The importance of the feed support struts, feed gain pattern, and surface distortions to the modelling of the side-lobe gain pattern of large antennas of the DSN and radio astronomy has been considered.

For a wide range of angles, the side-lobe level is dominated by scattering from the struts. For the side-lobes the accuracy of the treatment of struts is therefore the dominant factor.

At certain angles of view, spillover (radiation direct from the feed) can be a dominant factor. For many antennas, spillover produces the highest peak in the far-out side-lobe envelope. Generally, spillover is dominant in the range of 80° to 120°. Thus knowledge of the feed horn gain pattern, particularly at angles near the spillover angle, is an important parameter.

The distortions to the surface of the reflector can cause an increase in the level of the both near-in and far-out side lobes. The correlation length has a direct bearing on the increase. Smaller correlation length spreads the errors towards far-out side lobes, while larger correlation lengths focus the increase at near-in side lobes. The effect becomes more significant as the size of the surface errors increases in terms of the wavelength.